XX. Liquid Propulsion

PROPULSION DIVISION

A. High-Thrust Throttleable Monopropellant Hydrazine Reactors, *T. W. Price*

1. Introduction

Studies of rendezvous and landing missions have shown advantages for throttleable monopropellant hydrazine rocket engines to provide the terminal velocity correction. These thrusters would be used in much the same manner as the bipropellant vernier engines on JPL's *Surveyor* spacecraft. A requirement for a rocket with maximum thrust of 500 to 1000 lbf appears in several conceptual missions for unmanned spacecraft, the most immediate of which is the *Viking* Mars lander.

There are three primary factors which led to the choice of hydrazine, and all are related to the extra-terrestrial life experiments planned for the landing missions. These are: (1) the stagnation temperature of the hydrazine decomposition products is much lower than that from a bipropellant engine (2000°F compared to 5000°F for the N_2H_4–N_2O_4 system) and this reduces the likelihood of destroying soil organisms in the vicinity of the landing site, (2) heat sterilization of the complete propulsion system, including the fuel, before launch is feasible (SPS 37-47, Vol. III, pp. 153–162), and (3) the exhaust gases contain only small amounts of the two species[1], carbon and water, of most interest to the life scientists. The inherent, superior reliability of monopropellant propulsion systems, as compared to bipropellants, further enhances their desirability in spite of the lower specific impulse of the monopropellant.

Among the problem areas associated with large monopropellant reactors of this type, some would be expected, at least *a priori*, to be similar to those experienced with the *Mariner*-size engines. Chief among these would be catalyst retention, structural support of the catalyst and adequate distribution of the fuel over the catalyst bed. Lander mission requirements, such as sterilization and dynamic throttling, may pose additional problems. Although none of these problems appears insurmountable, only a limited amount of experience with either high thrust or throttled hydrazine reactors has been accumulated to date.

[1]Both are present as impurities (the carbon as aniline) and could be almost completely removed, if necessary.

Therefore, an applied research program to investigate the broad technology area of high-thrust throttleable monopropellant hydrazine engines is in progress. This program was divided into two major parts, both under JPL technical direction: a contracted effort with TRW Systems Group and an in-house effort at JPL. The contracted program has been completed. The results are the subject of a formal report (Ref. 1) prepared by TRW and will not be discussed here. The initial phase of the in-house program, two series of subscale tests, has been completed and is the subject of this article. For these tests, surplus *Mariner* Mars 1969 reactors, which provide 50 lbf of thrust in vacuum, were used. The subscale tests were directed at a fuller understanding of the effects of dynamic throttling and sterilization. Each series is discussed separately.

2. Dynamic Throttling Tests

a. Objectives. The primary objectives of this group of tests were to assess the problems involved in controlling a subscale throttle valve/reaction chamber by means of a signal pre-recorded on magnetic tape (in preparation for test with larger chambers) and to determine if there were any fundamental problems involved in dynamically throttling a hydrazine decomposition chamber. In addition, the subscale hardware used was of interest in itself for potential use on one version of a contemplated Jupiter orbiter spacecraft. Therefore, secondary objectives were the evaluation of the dynamic characteristics of the specific throttle valve/reactor combination and of the performance of the catalytic reactor at various throttle levels.

b. Apparatus and procedures. For the tests to be described, thrust chambers from the *Mariner* Mars 1969 program were mated with a throttle valve from the *Surveyor* program (Ref. 2). Surplus components were used throughout because of cost and availability considerations. The basic *Mariner* Mars 1969 engine configuration is shown in Fig. 1. An engine/valve combination, as set up for testing, is shown in Fig. 2.

Two comments are pertinent to the setup of Fig. 2. First, the hardware was originally assembled and supplied to the Langley Research Center for a series of soil contamination tests. The piping appears somewhat cramped because it was arranged so that the engine/valve assembly could be test-fired at JPL, packaged, and shipped with a minimum of disassembly. Second, the *Surveyor* propulsion system utilized both a fuel and an oxidizer; consequently, the throttle valve consists of two

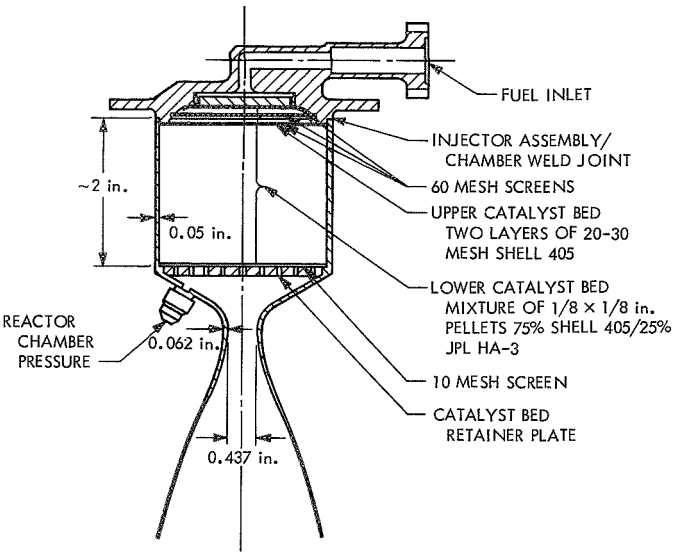

Fig. 1. *Mariner* Mars 1969 engine, internal configuration

variable area fluid systems, with both the fuel and oxidizer pintles being positioned by a single actuator. Neither of the two valve circuits by itself can accommodate the design flowrate (0.22 lbm/s) of the monopropellant reactor without an excessive pressure drop, but both sides in parallel are adequate. Therefore, the single hydrazine supply line is divided just upstream of the *Surveyor* valve (Fig. 2), hydrazine is routed to both parts of the valve, and the two lines are rejoined downstream of the valve. In addition, a normally open solenoid valve was placed in one of the two parallel lines so that flow through one side of the throttle valve could be remotely closed off. Thus, the range of flow rates possible with a single supply tank pressure was increased.

Two different reactors, of basically the same design, were used. For tests 4–6[2] and 23–26 engine SN C-101 was used. Engine SN B was employed for all other tests in this series. The significant dimensions and catalyst bed configuration were the same for both engines and are as shown in Fig. 1. The major difference between the two is that the injector of SN C-101 bolts to the chamber instead of being welded.

During the initial tests (numbers 4–6) the throttle valve position was controlled manually by means of a

[2]All tests are numbered sequentially regardless of the hardware being used. Thus, the first tests of these series do not begin with 1, and test numbers for the same hardware do not necessarily follow sequentially.

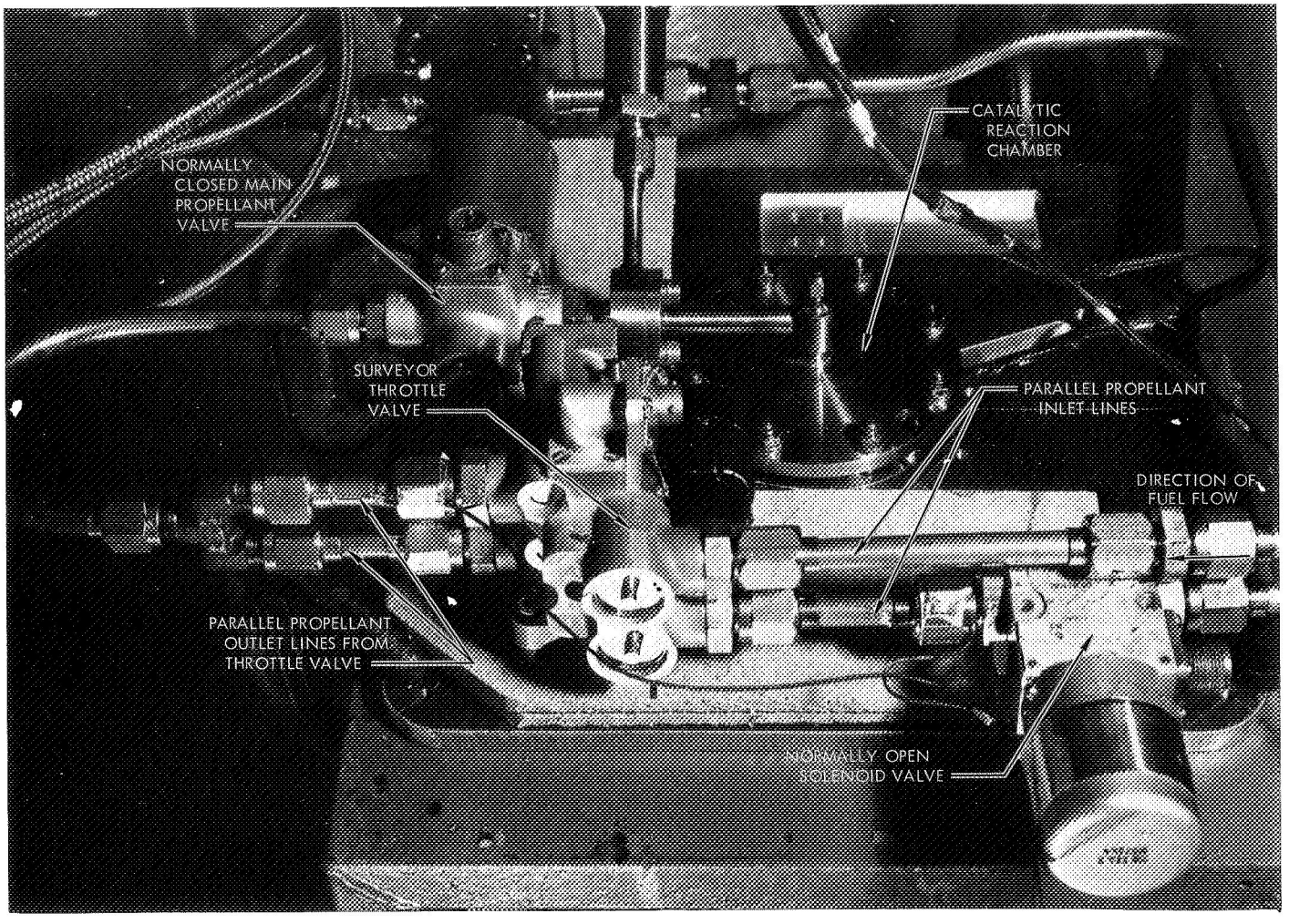
NORMALLY CLOSED MAIN PROPELLANT VALVE
CATALYTIC REACTION CHAMBER
SURVEYOR THROTTLE VALVE
PARALLEL PROPELLANT INLET LINES
DIRECTION OF FUEL FLOW
PARALLEL PROPELLANT OUTLET LINES FROM THROTTLE VALVE
NORMALLY OPEN SOLENOID VALVE

Fig. 2. *Surveyor* throttle valve for *Mariner* Mars 1969 engine ready for test

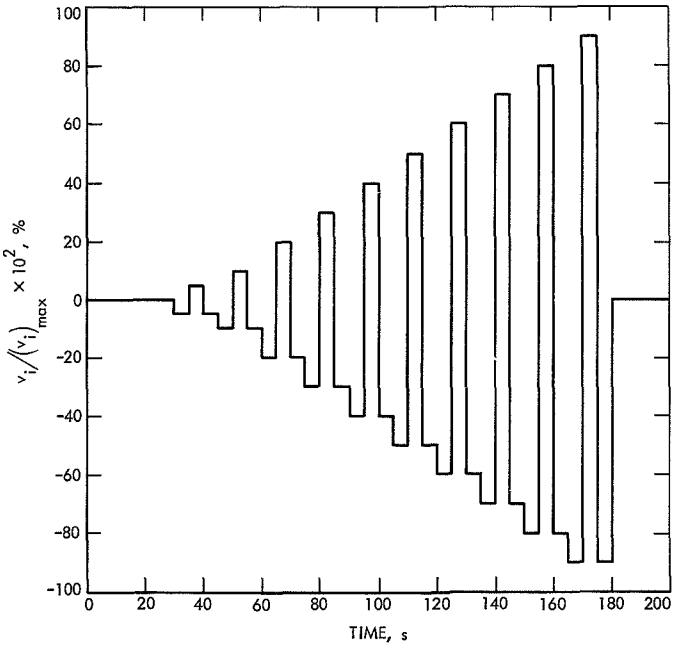

Fig. 3. Square wave duty cycle for throttle valve tests

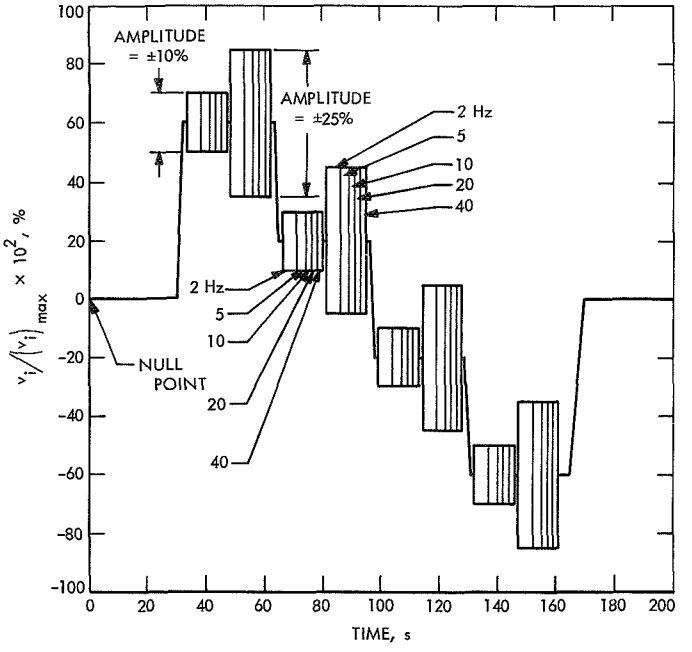

Fig. 4. Sinusoidal duty cycle

potentiometer. For the remaining tests (numbers 23–26 and 66–68) throttle valve control was from magnetic tape. The two duty cycles used for remote control of the throttle valve are shown in Figs. 3 and 4. The signals are expressed as the ratio of valve input voltage to the value of input voltage corresponding to the maximum travel in either direction about the null point. The throttle valve itself is designed so that at zero input voltage (i.e., the null point) the pintles are approximately halfway between the travel limits. Square and sinusoidal (two amplitudes and five frequencies about four different mean levels) signals were employed even though the idealized duty cycles of Figs. 3 and 4 would most likely not be employed during a mission. Rather, the response to such signals defines the system dynamic characteristics and provides data directly applicable to the design of the necessary control circuitry.

In addition to throttle valve position, the hydrazine supply tank pressure is another variable by which the absolute engine output level can be varied. The tank pressure was chosen so that with the valve in the null position the reactor pressure would be slightly under the nominal *Mariner* Mars 1969 operating pressure of 200 psia. Since one-half the valve stroke is above the null point, the fuel flow rate could be increased above that corresponding to the null position, and the engines operated at pressures above, as well as below, the design value. The *Mariner* Mars 1969 thrust chamber can be operated at 1.5 times the design pressures, so that such throttling was still well within the engine's capabilities.

c. Results and Discussion. The primary objectives of this test series were attained. Dynamic control of a throttle valve from a pre-recorded signal was demonstrated, and no problems in the rapid throttling of a hydrazine decomposition chamber were encountered. The response of the engine and valve to the step and sinusoidal signals was measured, but since the valve has no positive position indicator, the characteristics of the chamber cannot be separated from those of the valve, and the data are applicable only to the specific valve/chamber combination tested.

The planned test sequence for the square-wave input of Fig. 3 was to repeat this duty cycle three times without an engine shutdown between repetitions. This was chosen as grossly representative of the duty cycle for the contemplated Jupiter orbiter spacecraft. Because of a minor facility problem a shutdown was required just before completion of the first cycle. (Thus, test 66 was slightly shorter than either tests 67 or 68.) After correction of the problem, tests 67 and 68 were completed as originally planned.

The results of the step input tests (66, 67, and 68) are presented in Figs. 5 through 8. Figures 5 and 6 are tracings from an oscillogram and show behavior during

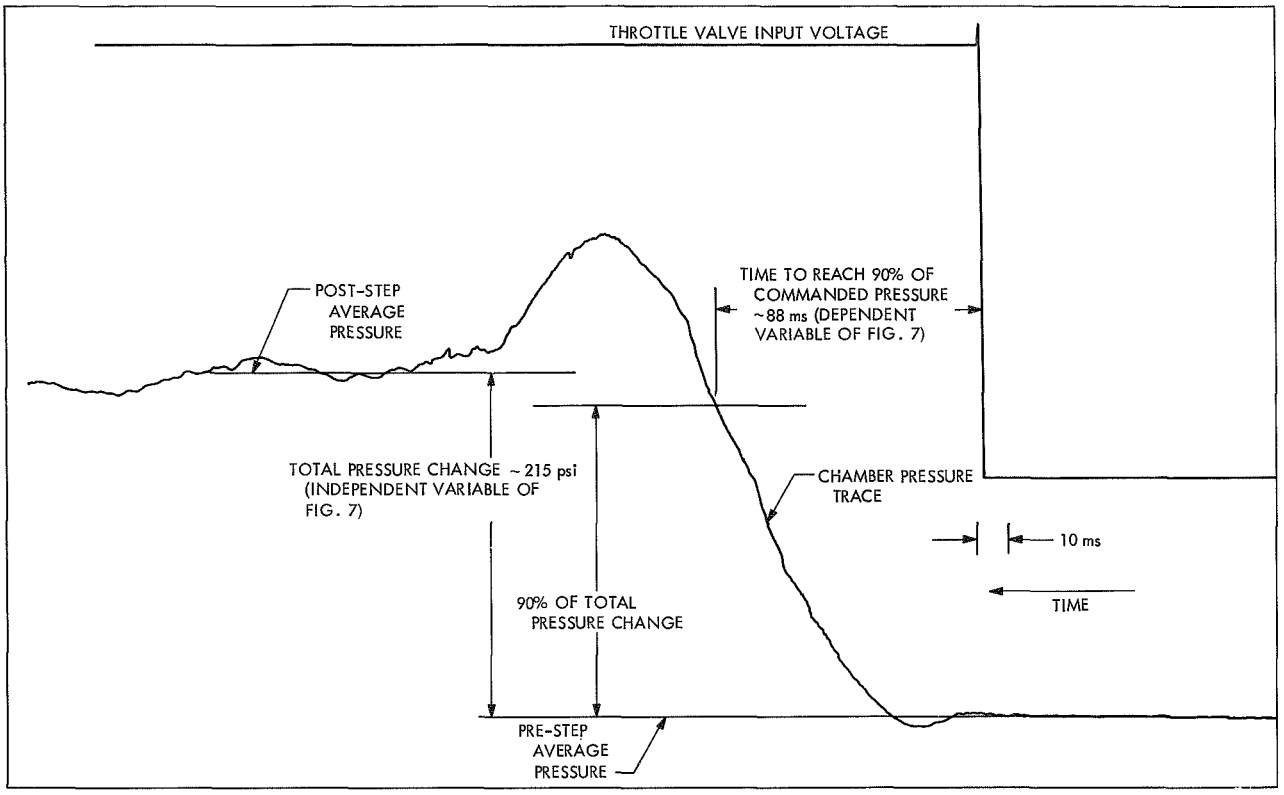
THROTTLE VALVE INPUT VOLTAGE
POST-STEP AVERAGE PRESSURE
TIME TO REACH 90% OF COMMANDED PRESSURE ~88 ms (DEPENDENT VARIABLE OF FIG. 7)
TOTAL PRESSURE CHANGE ~215 psi (INDEPENDENT VARIABLE OF FIG. 7)
CHAMBER PRESSURE TRACE
10 ms
TIME
90% OF TOTAL PRESSURE CHANGE
PRE-STEP AVERAGE PRESSURE

Fig. 5. Typical "up-throttle" step

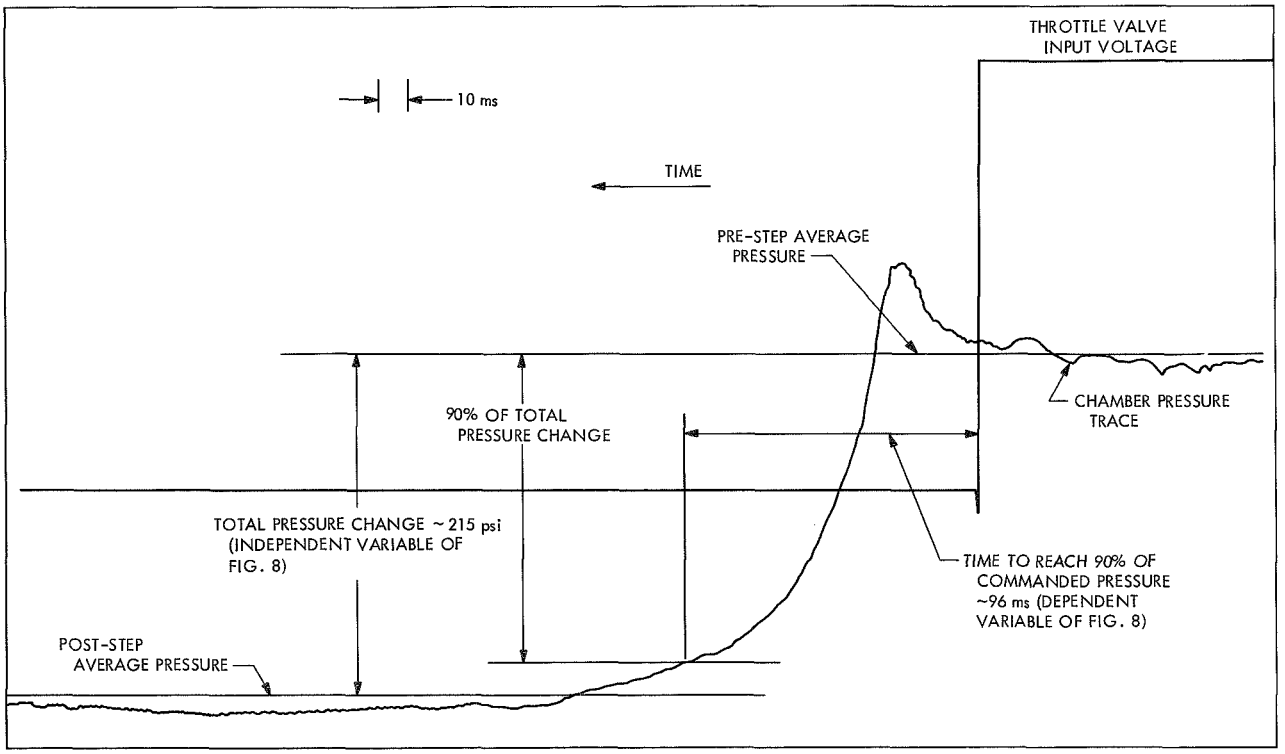
THROTTLE VALVE INPUT VOLTAGE
10 ms
TIME
PRE-STEP AVERAGE PRESSURE
CHAMBER PRESSURE TRACE
90% OF TOTAL PRESSURE CHANGE
TOTAL PRESSURE CHANGE ~215 psi (INDEPENDENT VARIABLE OF FIG. 8)
TIME TO REACH 90% OF COMMANDED PRESSURE ~96 ms (DEPENDENT VARIABLE OF FIG. 8)
POST-STEP AVERAGE PRESSURE

Fig. 6. Typical "down-throttle" step

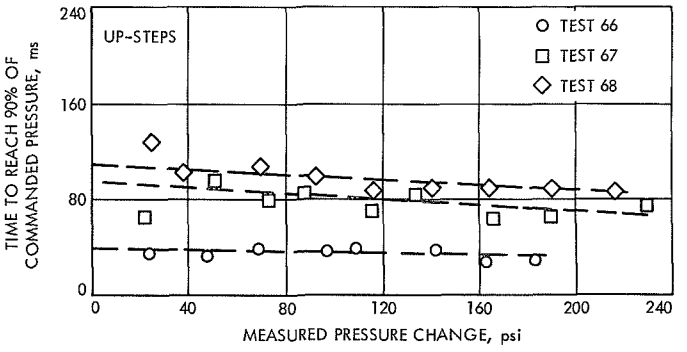

Fig. 7. Response to pressure increase

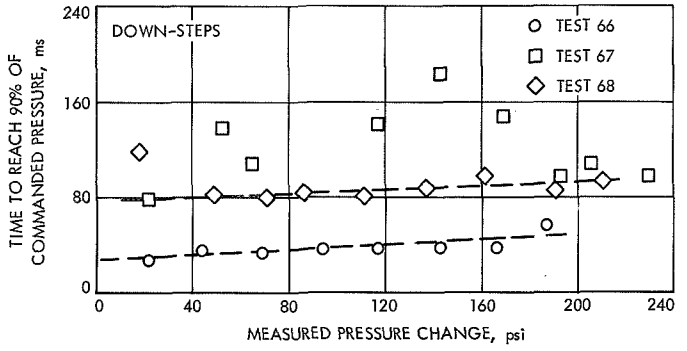

Fig. 8. Response to pressure decrease

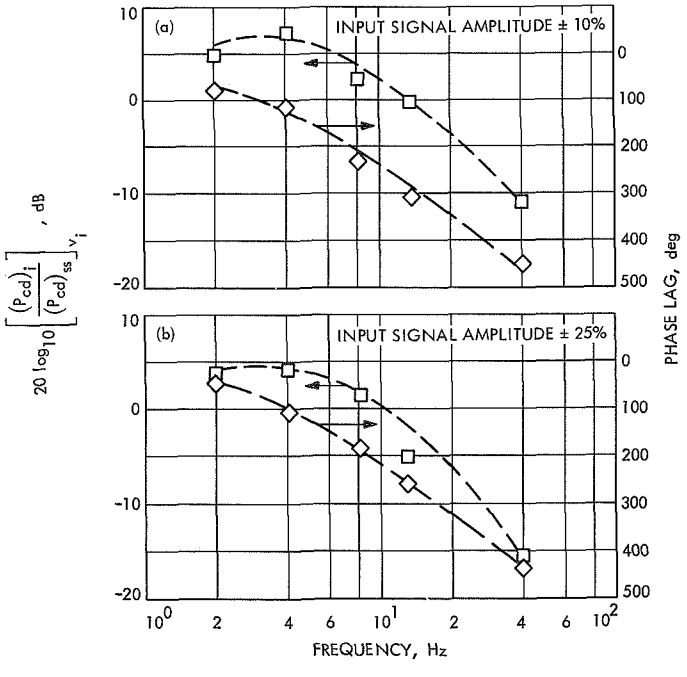

Fig. 9. Amplitude ratio and phase lag versus frequency input signal: (a) amplitude ±10%, (b) amplitude ±25%

a typical "up-step" and "down-step," respectively. Also defined on Figs. 5 and 6 are the total chamber pressure change resulting from the step input, and the time required to reach 90% of this value. These two variables are correlated for all three tests in Figs. 7 and 8.

Figures 7 and 8 are plots of the engine/valve response time versus the pressure change. As used here the response time is defined as the time increment from a change in the valve command signal until the chamber pressure reaches 90% of the final steady-state value (Figs. 5 and 6). The pressure change is simply the difference between the initial and final steady-state reactor chamber pressures. The straight lines of Figs. 7 and 8 were fit to the data by a least-squares method. No attempt was made to fit a curve to the data from the down-throttle step of Test 67 (Fig. 8), because of its erratic nature. The response times are nearly independent of the size of the pressure steps within each test, but there was a substantial increase in the level of response times between tests 66 and 67. Neither the cause of this change nor the source of the erratic data from the down throttle steps of test 67 have yet been determined.

By way of comparison, the response requirement for the contracted effort with TRW was 75 ms. This requirement is moderately difficult, but within the current state-of-the-art, and is representative of the *Viking* requirement. The *Mariner* engine/*Surveyor* valve easily met the 75 ms during test 66, marginally during test 67, and not at all during test 68. Such shifts in response would be unacceptable in a flight application. Because of the lack of a positive valve position indication these response changes cannot be ascribed with certainty to either the chamber or valve. The same effect will be searched for during the full-scale testing to be conducted, and, if observed, the source should be determined since the larger throttle valves are equipped with positive position transducers.

Typical engine/valve response to the sinusoidal input (Fig. 4) are shown in Fig. 9 as standard Bode plots. Figure 9a illustrates the response to an input signal amplitude of ±10%, while Fig. 9b shows the response for ±25%. Because of the quantity of data gathered not all was reduced and plotted. The phase lag of Fig. 9 is defined as the time between identical positions (e.g., maximum points) on the recorded throttle valve command signal and the reactor chamber pressure oscillo-

gram traces and is expressed in degrees. The amplitude ratio is defined as

$$20 \log_{10} \left[\frac{(P_{cd})_i}{(P_{cd})_{ss}} \right]_{vi}$$

in decibels, where $(P_{cd})_i$ and v_i are point values of reactor chamber pressure and throttle valve input voltage, respectively, and are evaluated at any arbitrary point during the sinusoidal period. $(P_{cd})_{ss}$ is the reactor chamber pressure that would result from the application of v_i to the valve under steady-state conditions. The steady-state relationship between P_{cd} and v was determined from tests 66 to 68, described above.

Note that the data resulting from the ±10% amplitude input signal show a greater phase lag and larger amplitude ratio than that resulting from the ±25% input signal. This is as one might expect. The larger amplitude signal requires a greater mechanical movement of the valve in the same time period, and hence inertia effects are greater. Similarly, greater changes in the propellant flow rate are required, so that flow inertia effects are also greater. The valve/chamber/propellant feed system exhibits less damping when subjected to the lower amplitude input signal.

Again, for the purposes of comparison, the sinusoidal response requirement used in the TRW contract was, that in response to a sinusoidal throttle valve input signal of 5 Hz and amplitude of ±10%, the thrust should have a phase lag no greater than 45 deg and the amplitude ratio should be greater than or equal to 0.7 (footnote 3); i.e., less negative than −3.1 dB, or even positive. From Fig. 9 it is clear that the *Mariner* engine/*Surveyor* valve combination could not meet the moderate phase lag limits, but could satisfy those for the amplitude ratio. However, included in the specifications for any flight system would probably be an *upper* limit on the amplitude ratio. A value of +0.2 dB would be typical. Such limitation of amplification might also prevent the present engine from meeting the flight criteria at 5 Hz, as may be seen from Fig. 9.

[3]The contract requirement is in terms of a thrust ratio, F_i/F_{ss}. Since thrust is directly proportional to reactor chamber pressure, $(F_i/F_{ss} \cong P_i/P_{ss})$ the 0.7 figure can be converted to decibels by the relationship above. The equivalent value is −3.1 dB.

Included within all the duty cycles, both manually and remotely controlled, were many periods of relatively short, but steady-state operation. From this steady-state operation it is possible to determine the reactor performance at various throttle conditions. This type of data is needed for control of a landing maneuver. Given the spacecraft altitude, velocity, and acceleration, a throttle valve position can then be chosen to yield a thrust that will, in turn, result in a "soft" landing. The steady-state reactor performance, as measured by the characteristic velocity (one of the classical indices of rocket performance), is summarized in Fig. 10. Data from all the tests in this series are included there.

Also included on Fig. 10 are the performance predictions derived from Refs. 3, 4, and 5. Given the reactor geometry, fuel flow rate, chamber pressure, and the catalyst particle size and distribution, these references predict the composition of the gases leaving the catalyst bed. For monopropellant hydrazine the theoretical characteristic velocity is a unique function of the gas composition. Thus, for a given reactor, c^* as a function of mass flow rate can be predicted. Experimental c^*s are generally a large fraction of the theoretical values since catalytic reactors are not nearly as susceptible to mixing and atomization losses as are bipropellant injectors. However, while the predictions from Refs. 3, 4, and 5 are in reasonable agreement among themselves[4], none predict the observed performance degradation at the lower flow rates evident in Fig. 10.

Since all three referenced correlations are based on data taken at bed loadings as low as 0.1 (lbm/(in.^{2}-s) it is concluded that the present performance degradation, as well as the erratic nature of the data at such low flow rates, result from a source other than excessive ammonia dissociation. Although it is known that propellant atomization is less important for hydrazine catalytic reactors than for a bipropellant engine, it is hypothesized that this may be the source. This same problem was not observed by TRW (Ref. 1) during the very limited amount of testing they completed with a 600-lbf-thrust

[4]Note that Ref. 5, strictly speaking, is not applicable to the Shell 405 catalyst used in these tests. Comparison between the correlation of Ref. 5 and the present data was attempted, however, because of the lack of agreement between experiment and the theories of Refs. 3 and 4 at low flow rates. As expected, Ref. 5 predicts a higher c^*, but again the dependence on $\dot{m}$ is slight and of the same order of magnitude as in the other two works.

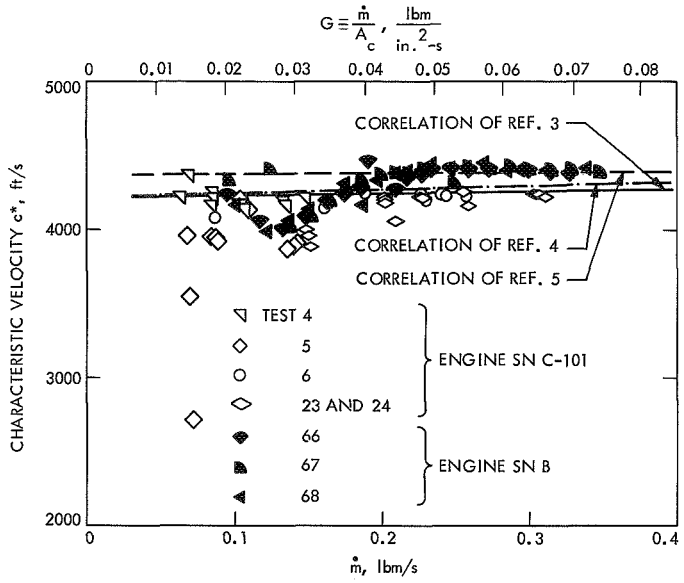

Fig. 10. Steady-state performance of *Mariner* Mars 1969 engine as a function of flow rate

engine. This phenomenon will be investigated further in future work.

3. Heat Sterilization Tests

a. Objective. In order to significantly reduce the possibility of introducing terrestrial organisms to another planet, all spacecraft which might impact or are intended to soft-land must be sterilized. Heat sterilization is the method most often used. The vehicle must be subjected to six 64-h periods at 275°F in a nitrogen atmosphere. Since a hydrazine decomposition chamber typically operates at temperatures of about 2000°F, there is no reason to expect that the sterilization requirements outlined above should significantly change an engine's operating characteristics. A short series of reactor tests was conducted to verify this.

b. Apparatus and procedures. The following steps were followed in the sterilization investigation. Two surplus *Mariner* Mars 1969 flight engines, numbers SN 005 and SN 008, were used for these tests. SN 005 was sterilized, while SN 008 served as a control. Since the engines had slightly different test histories, they were first repacked with fresh catalyst. The repacking was accomplished by machining open the engines at the injector-chamber weld joint (Fig. 1), filling both the upper and lower beds with unfired catalyst (the same size and types were used as shown in Fig. 1), and then rewelding. Each engine was then test-fired continuously for 45 s at fixed thrust before sterilization, so as to obtain baseline performance measurements. The tests were made as identical as possible by conducting both on the same day, using hydrazine from the same lot, using the same instrumentation, etc. Following the baseline tests, all propellant and instrumentation openings of engine SN 008 were capped, the nozzle exit was covered with tape, and the engine was stored in its wooden transportation container. Engine SN 005 was sterilized in the materials research process laboratory at JPL. The temperature–time schedule noted above was followed. After the sterilization, which required 19 days to complete, all openings of engine SN 005 were closed in the same manner as for SN 008, and the engine returned to the test cell. The fixed-thrust performance tests were then repeated, again under identical conditions.

c. Results and discussion. Three criteria were used to judge the effect of heat sterilization on reactor operation. These were: (1) the characteristic velocity, c^*, (2) roughness, as measured by the normalized chamber pressure fluctuations, $\Delta P_{cd}/2P_{cd}$, and (3) the start transient characteristics, such as ignition delay (the time between the electrical signal to open the propellant valve and the first indication of chamber pressure), pressure rise time (the time between the first indication of chamber pressure and the attainment of 90% of the final steady-state pressure), and the peak overpressure (the maximum pressure attained during the start transient). The results of the four tests are summarized in Table 1.

Only the start transient characteristics exhibited a noticeable change. The ignition delay and pressure rise times both increased noticeably. The overpressure in itself is not considered particularly significant, since it is a direct result of the increased ignition delay and pressure rise-time. The fuel flow rate is fixed by the pressure drop across the injector, and since this pressure differential is large until chamber pressure is built up, the fuel flow rate is also large during the ignition delay/pressure rise-time periods. The net result is that the reactor fills with a gas mixture which is largely vaporized, unreacted hydrazine. Once ignition is achieved, this hydrazine reacts very rapidly, and hence the overpressure. Similar sterilization tests in which no overpressure was noted were subsequently conducted at TRW and are reported in SPS 37-47, Vol. III. However, the test setup used there included a throttle valve incorporating a cavitating venturi which prevented the fuel flow rate from going above the final steady-state value and thus reduced the quantity of fuel accumulated in the chamber.

Table 1. Summary of results of heat sterilization experiments

Test No.	Engine No.	P_c (avg), psia	$\dot{m}$, lbm/s	c^*, ft/s	$\frac{\Delta P_{cd}}{2P_{cd}}$	Ignition delay, ms	Peak pressure, psia	Pressure rise time, ms
21	SN 005	206.8	0.234	4360	2.4	98	245	67
22	SN 008	187.6	0.214	4320	2.0	100	206	50
37	SN 008	189.8	0.216	4310	1.9	129	204	60
38	SN 005[a]	206.9	0.234	4370	2.0	159	454	85

[a]After sterilization.

The details of the start transient of a catalytic monopropellant hydrazine engine are not well understood at the present; in fact, this process is the subject of a JPL-managed NASA Advanced Technology Contract (Ref. 6). Work done under that contract shows that the catalyst activity may be reduced when it is exposed at elevated temperatures to an inert gas, such as nitrogen. However, the activity reduction is reversible and has no discernible effect on steady-state operation. For a planetary lander application such as *Viking*, where the engine control is through an active guidance system, this initial pressure overshoot should cause no great problem, since the additional impulse can be compensated for later in the mission. However, for a passive, preprogrammed engine firing duration this could be a more significant problem. Such passive control has been used on all the JPL *Mariner* missions completed to date, and is currently planned for the *Mariner* Mars 1973 spacecraft.

Based on present results and those of other workers, it is reasonable to conclude that heat sterilization has a significant effect on only subsequent reactor start transient characteristics.

Definition of terms

A_c cross-sectional area of the cylindrical chamber, in.^{2}

A_t area of nozzle throat, in.^{2}

c^* characteristic velocity $\equiv \frac{P_{cd} A_t g_0}{\dot{m}}$, ft/s

g_0 units conversion factor; numerically equal to $32.174 \frac{\text{lbm-ft}}{\text{lbf sec}^2}$

F thrust, lbf

G catalyst bed loading $G \equiv \frac{\dot{m}}{A_C}$, lbm/in.^{2}-sec

$\dot{m}$ propellant mass flow rate, lbm/sec

P_{cd} reactor chamber pressure measured downstream of the catalyst bed (Fig. 1), lbf/in.^{2}

ΔP_{cd} average amplitude of fluctuations in chamber pressure about their mean value, lbf/in^2

v_i valve input emf, V

$(v_i)_{\max}$ value of v_i corresponding to maximum valve travel, in either direction, about the null position, V

References

1. Kenney, R. J., and Reeves, D. F., "Throttleable Thruster System," Final Report, JPL Contract 952344, TRW Report No. 70-4726.3-28, April 28, 1970.

2. *Surveyor Project Final Report, Part 1. Project Description and Performance, Vol. II*, Technical Report 32-1265, Jet Propulsion Laboratory, Pasadena, Calif., July 1, 1969.

3. "Development of Design and Scaling Criteria for Monopropellant Hydrazine Reactors Employing Shell 405 Spontaneous Catalyst," Final Report, NASA Contract NAS 7-372, Rocket Research Corp. Report RRC-66-R-76-Vol. II, Jan. 18, 1967.

4. Kesten, A. S., "Analytical Study of Catalytic Reactors for Hydrazine Decomposition," Second Annual Progress Report, NASA Contract NAS 7-458, United Aircraft Research Laboratories Report No. UARL G910461-24, May 1968.

5. Grant, A. F., Jr., "Basic Factors Involved in the Design and Operation of Catalytic Monopropellant-Hydrazine Reaction Chambers," Report 20-77, Jet Propulsion Laboratory, Pasadena, Calif., Dec. 31, 1954.

6. Sangiovanni, J. J., and Kesten, A. S., "Study of Hydrazine Reactor Vacuum Start Characteristics," First Annual Progress Report for NASA Contract NAS 7-696, United Aircraft Research Laboratories Report No. UARL H910758, December 1969.

B. Injector Hydrodynamics Effects on Baffled-Engine Stability—A Correlation of Required Baffle Geometry With Injected Mass Flux,

R. M. Clayton

1. Introduction

It is well known that baffles can inhibit the development of sustained high-amplitude transverse wave systems in liquid rocket combustion chambers. Further, research conducted by JPL and others indicates that for conventional high-performance combustors, baffles are found to be most effective when placed in the early reaction region near the injector. Thus it can be argued that a primary variable, controlling baffle effectiveness, is the spatial relationship of the baffle geometry with the distribution of unreacted propellants. However, there are virtually no design criteria to reliably prescribe the necessary baffle/combustion-distribution relationship to provide a high margin of stability against resonance-initiating disturbances imposed either artificially or spontaneously.

The effective axial length of the early reaction region presently remains difficult to define for any given combustor because of the complexities of the overall combustion process; but it is clear that liquid phase atomization and propellant distribution largely determine the eventual combustion distribution, and that these properties are injector performance variables. Moreover, any substantial response of injector performance to perturbed combustion chamber conditions can, in general, only further complicate the dynamic behavior of the overall combustor. This responsiveness is believed to exist for most dynamic stability experiments with the conventional flight-type injectors for which other system requirements usually dictate minimized injector pressure drops. Thus, correlation of stability testing results, in terms of injector design variables, historically has been nearly impossible, and trial and error methods for injector "fixes" have prevailed.

In contrast, the JPL resonant combustion research has emphasized injection schemes producing steady reproducible hydrodynamic properties by virtue of the high flow-impedance and developed flow characteristics of long-tube (length = 100 D) orifices. Hence, the hydrodynamic boundary conditions governing spray formation have been controlled so that meaningful correlations should be possible between injector performance variables as "causes" and observed combustor behavior as "effects." Invariably, combustors using these JPL injectors have exhibited a low dynamic-stability margin without baffles (i.e., stable to ordinary low levels of combustion noise, but unstable to discrete disturbances) producing a fully developed spinning detonation-like wave described in Ref. 1. But just as invariably, they have been reliably stabilized with baffles without modifications to the injection schemes. This stabilization procedure is contrary to nearly all contemporary flight engine development histories.

The observations stated above have led to a JPL conclusion that the essential qualitative requirement for maximizing the stability control effectiveness of baffles is as follows: provide sufficient hydrodynamic control of the injected flow so that the spatial distribution of mass and energy sources in the early reaction region is reproducibly compact and steadily maintained, relative to the baffle geometry, under perturbed combustion conditions.

For the conclusion to be very useful, however, it is presumed to be necessary to quantize two important criteria: (1) the critical spatial relationship between baffle geometry (length and spacing) and a fixed combustion distribution, and (2) the lower limit of control over the injection hydrodynamics required to maintain that critical spatial relationship in the presence of high amplitude combustion disturbances. The latter design limit information is important for minimizing possible design complications associated with long orifices while at the same time providing the lower limit of compromise to hydrodynamic control. Consequently, an investigation seeking these criteria was initiated with the intent of using combustion hardware from previous studies and a new "variable-control" injector. However, funding limitations have forced a termination of the investigation (first reported in SPS 37-62, Vol. III, pp. 272–279), and further work is expected to be delayed for an indefinite time.

This article presents the results of a final series of experiments before work was terminated that concern the first criterion itemized above and compares them with results from previous experiments. It will be shown that a correlation between baffle geometry and at least one injector performance variable is demonstrated and that this correlation can be stated in terms of rudimentary design criteria. The correlation holds, hence the design criteria is valid even though the relationship does not yet include terms that represent the combustion distribution specifically.

2. Description of Experiments

The dynamic stability of the baffled long-tube research injector, RMIR-5, was determined in order to supplement existing data for two other JPL injectors having similar stiff hydraulic configurations: injector RC-1 (SPS 37-62, Vol. III, pp. 272–279); and injector RMIR-7 (Ref. 2). Other design characteristics common to the respective combustors are uniform average mass flux distributions (non-humped distributions), unlike doublet injection elements, and cylindrical chambers nominally 16 in. (41 cm) long with an area contraction ratio of 2.0. Nominal values of design and operational differences for each combustor are listed in Table 1. Specific injection scheme variables are listed in Table 2.

Both 3 and 5 blade baffle arrays were used with the 11-in. (28 cm) diam RMIR-5 combustor. Blade lengths ranging from 1.5 to 7.8 in. (3.81 to 19.81 cm) were investigated for the three-blade array, and lengths of 2.0, 2.9, and 4.0 in. (5.08, 7.37, and 10.16 cm) were used for the five-blade array. These configurations are shown in Fig. 1, where they can be compared with the RC-1 and RMIR-7 arrays used previously. For all of the experiments, the blades were welded to the injector face and were hand fitted so that no significant end gap (not more than several thousands of an inch) existed at the chamber wall. The somewhat nonradial placement of the blades was dictated by available space within the orifice arrangements of the respective injectors. The generally nonsymmetrical circumferential spacing stemmed partially from the same consideration, but also from intuitive (and unproven) reasoning that gas motion coupling between baffle cavities would be reduced by the nonsymmetry.

The stability of the RMIR-5 engine was evaluated using an explosive-bomb technique. The effectiveness of each length baffle was tested by imposing bomb discharges of various sizes [2, 6.9, 13.5 gr (0.13, 0.45, 0.87 mkg) of PETN in the form of electrically initiated blasting caps] from various chamber locations. In practice, as

Table 1. Combustor operating conditions (nominal values for design conditions)

	RMIR-5	RC-1	RMIR-7
Propellants	SFNA + *Corporal* fuel[d]	N_2O_4 + 50/50 (UDMH/N_2H_4)	N_2O_4 + N_2H_4
Overall mixture ratio r	2.80	2.00	1.20
Main mixture ratio r_m	2.80	2.11	1.20
Boundary mixture ratio r_b	None	1.27	None
Total propellant flowrate $\dot{m}_t$, lbm/s (4.54 × 10^{-1} kg/s)	95.8	79.4	83.5
Mass fraction of boundary flow, $\dot{m}_b/\dot{m}_t$	—	0.10	—
Average chamber mass flux $\bar{G}_{ch}$, lbm/s-in.^{2} (7.04 × 10^2 kg/s-m^2)	1.01	0.31	0.88
Chamber pressure, psia (6.89 × 10^3 N/m^2)	300	100	300
Chamber diameter, in. (2.54 cm)	11.04	18.04	11.04
Combustion efficiency[a], %	97	97	96
Combustion roughness, psi rms (6.89 × 10^3 N/m^2)	2.5	<1.0	15.0
Acoustic velocity[b], ft/s (3.05 × 10^{-1} m/s)	3500	3960	4030
Measured frequency of spinning tangential wave (without baffles), Hz	2120	1445	2420
Measured maximum amplitude of sustained spinning wave (without baffles)[c], psi p/p (6.89 × 10^3 N/m^2)	~2490	~750	~1000

[a]Based on ratio of measured to theoretical equilibrium c*.

[b]Based on measured c*.

[c]From Kistler measurements near injector "corner" of chamber.

[d]SFNA (*stabilized fuming nitric acid*) consists of a mixture of the following compounds with percentage by weight as noted: 81.3–84.5% HNO_3; 14.0 ± 1.0% NO_2; 2.5 ± 0.5% H_2O; 0.6 ± 0.1% HF.

Corporal fuel consists of a mixture of the following compounds with percentage by weight as noted: 46.5 ± 0.2% furfuryl alcohol ($C_4H_3OCH_2OH$); 7.0 ± 0.2% N_2H_4; 1.5% max H_2O; 0.7% max impurities; remainder, aniline ($C_6H_5NH_2$).

Table 2. Injection conditions (nominal values)

Condition	RMIR-5	RC-1[c]		RMIR-7
		Main flow	Boundary flow	
Number of elements	52	84	24	47
Oxidizer orifice diameter D_{ox}, in. (2.54 cm)	0.173	0.142	0.073	0.173
Fuel orifice diameter D_f, in. (2.54 cm)	0.0986	0.101	0.073	0.173
Oxidizer injection velocity V_{ox}, ft/s (3.05×10^{-1} m/s)	86.5	58.0	68.0	64.2
Fuel injection velocity V_f, ft/s (3.05×10^{-1} m/s)	137.6	86.0	92.0	73.5
Element flow rate ($\dot{m}_{el}$), lbm/s (4.54×10^{-1} kg/s)	1.84	0.85	0.33	1.81
Impingement distance from face, in. (2.54 cm)	0.75	0.625	0.125	0.75 or 0.875
Included impingement angle, deg. (1.75×10^{-2} rad)	44	60	60	45
Normalized peak mass flux sampled for element $(G_{max})_{SN}$[a], (lbm/s-in^2)/(lbm/s), [(1.55×10^3 kg/s-m^2)/(kg/s)]	0.232	0.104	Not determined	0.342
True angular location of peak mass flux (σ)[a], deg (1.75×10^{-2} rad)	4.78	0.0	Not determined	0.0
Mixing factor (η_m)[a], %	85.0	88.7	80.0	73.7
Mass median drop diameter for fuel ($\bar{D}_f$)[b], μm	466	392	330	712

[a]From nonreactive flow measurements described in Ref. 4.

[b]Based on correlations from Ref. 6: $\bar{D}_f = 10^5 \left(\frac{D_f^{0.27}}{V_f^{0.74}} \frac{D_{ox}^{0.023}}{V_{ox}^{0.33}} \right) (K_p)(K_\alpha)$

where K_p = correction for physical properties

K_α = correction for impingment angle

[c]Mass flux correlations shown in Fig. 6 based on main flow elements.

many as six bombs of a selected size were discharged sequentially, nominally 100 ms apart, during each engine firing. Bomb locations, order of firing, and construction details were essentially the same as for the RC-1 experiments (SPS 37-62, Vol. III) and will not be repeated here. The RMIR-7 experiments did not use the bombs, but this combustor (using N_2O_4–N_2H_4) characteristically exhibits extremely noisy combustion and is spontaneously unstable to these abnormally high combustion disturbances when not equipped with baffles (Ref. 2). Thus, it is assumed that these spontaneous disturbances are equivalent to artificially imposed disturbances for the purpose of testing the combustor's dynamic stability with various baffle configurations.

Provisions for Photocon or Kistler measurements were available for all firings. Pertinent location information is specified where necessary as the results are presented. The physical and performance details of these measurement systems are described in Ref. 1.

The RMIR-5 injector was operated near its design mixture ratio of 2.80 (Table 1) for SFNA + *Corporal* fuel for most of the runs ($2.69 < r < 2.82$); however, inadvertent off-mixture ratios as low as 2.39 were observed for some firings. In view of the lack of sensitivity of baffle effectiveness to operating mixture ratio exhibited by RC-1 (SPS 37-62, Vol. III), these off-mixture ratio firings are not considered to influence the present results. The RMIR-7 data to be shown were also for near design conditions.

As with mixture ratio, total flow rate for the RMIR-5 experiments was held nominally constant for most firings at between 92.0 and 96.7 lbm/s (41.7 and 43.9 kg/s) producing a mean chamber pressure range of 292 to 307 psig (2.01 to 2.12 MN/m^2) at the injector face. Again, several firings inadvertently extended beyond this nominal range but are not considered sufficiently off-nominal to modify the results. Under these near-design flow conditions, c^* performance (corrected for stagnation pressure, but uncorrected for heat losses) was consistently 97% of theoretical equilibrium flow. Steady state combustion noise was generally less than 3 psi (20.7 kN/m^2) RMS with no tendency for popping. Analogous performance characteristics for the RC-1 and RMIR-7 combustors are summarized in Table 1 for comparison.

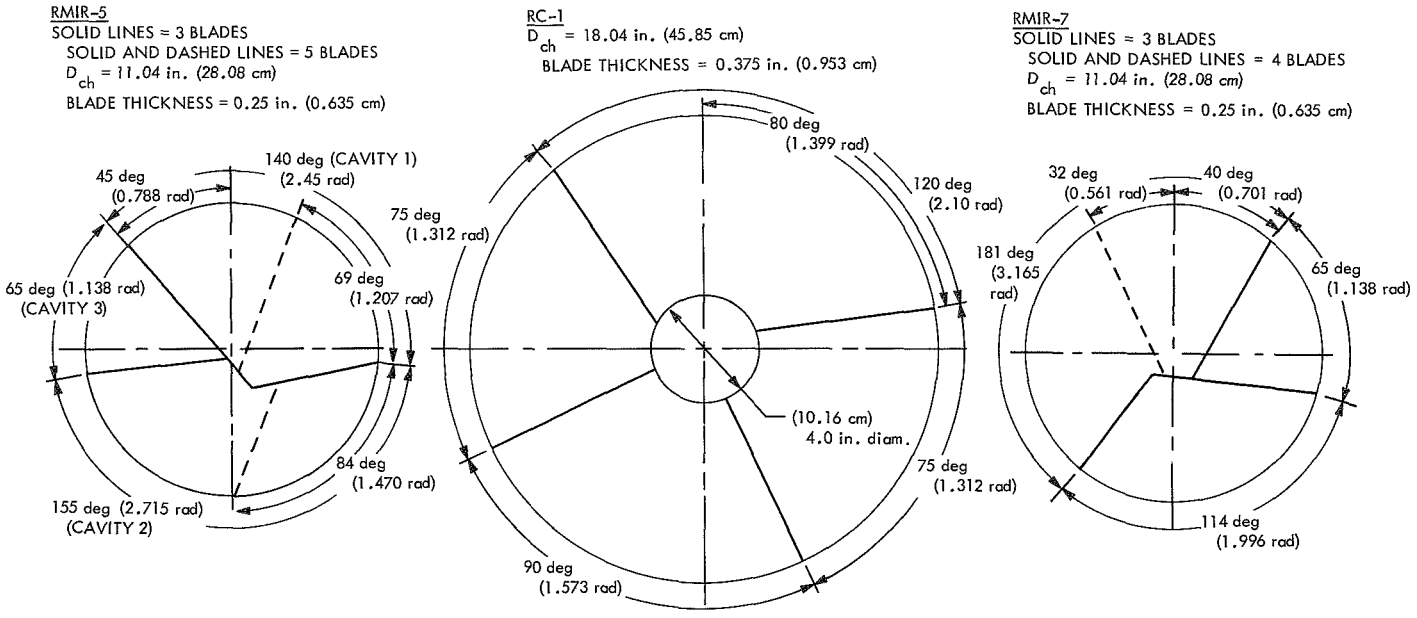

Fig. 1. Baffle array schematics for injectors RMIR-5, RC-1, and RMIR-7

3. Results for RMIR-5 Combustor

The overall results showing the dynamic stability characteristics of the RMIR-5 engine are summarized in Table 3. The engine was classified stable if for the particular baffle configuration all bomb disturbances damped with no discernible tendency for resonance at a sustained amplitude. Only the 5-blade array with lengths $\geq$2.9 in. (7.37 cm) were found to provide a high stability margin. For these stable configurations bomb pulse amplitudes between 165 and 1240 psi (1.14 and 8.55 MN/m^2) above mean chamber pressure, depending upon bomb and pressure measurement location, were damped after ~16 ms with a spread of 12 to 22 ms. The higher pulse amplitudes and longer damping times were associated with bombs located within the baffle cavities. Note that the rather large incremental length variations for the 5-blade array do not resolve the minimum length required by less than 0.9 in. (2.3 cm); therefore, the minimum length probably falls between 2.0 in. (5.08 cm) which was unstable and the 2.9 in. (7.37 cm) length which was stable.

For the 3-blade array, lengths in the range of 2.9 to 3.4 in. (7.37 to 8.64 cm) provided marginal stability in that the 2-gr (0.13 mkg) bomb damped (average damping time 12 ms) but the 6.9 and 13.5 gr (0.45 and 0.87 mkg) bombs did not in all cases. Thus, a lower level of stability was provided by the most effective 3-blade configuration compared to the most effective 5-blade array. Pulse amplitudes ranged 75 to 475, 100 to 720, and 160 to 610 psi (0.52 to 3.28, 0.69 to 4.96, and 1.10 to 4.21 MN/m^2), respectively, for the 2, 6.9, and 13.5-gr (0.13, 0.45, and 0.87 mkg) bomb pulses that did damp for this 0.5 in. (1.27 cm) range of baffle length. Bombs located within the baffle cavities were generally the most apt to initiate resonance when stability was marginal.

Lengths of the 3-blade array shorter than 2.9 in. (7.37 cm) did not provide stability to all 2-gr (0.13 mkg) bombs [amplitudes 135 to 390 psi (0.93–2.69 MN/m^2)]. Lengths greater than 3.4 in. (8.64 cm) were not all tested with the smallest bomb, but the results (Table 3) suggest that the greater lengths produced only marginal stability because they did not dampen all of the 13.5-gr (0.87 mkg) bombs [pulse amplitudes ranging from 65 to 735 psi (0.45 to 5.07 MN/m^2)].

The amplitudes quoted above are for pulses that *did* damp. Those pulses that *did not* damp were generally of substantially greater amplitude. For instance, one 13.5 gr (0.87 mkg) bomb pulse that failed to damp for a 3.4-in. (8.64 cm) baffle length was detected at 1690 psi (11.65 MN/m^2) even though the bomb was located 10.8 in. (27.4 cm) downstream of the injector. All pressures quoted above were measured by three Photocon transducers located circumferentially at a chamber station 4.0 in. (10.2 cm) from the injector face.

The resonance mode observed for the 5-blade array with the 2.0-in. (5.08 cm) length was a first tangential

spinning wave with a maximum amplitude of about 400 psi (2.76 MN/m^2) peak-to-peak and a frequency of 1735 Hz. This mode is termed a chamber mode herein because the baffle cavities as well as the chamber volume downstream of the cavities exhibited the same frequency. This exhibition of chamber modes rather than distinct baffle cavity modes was also noted for the RC-1 combustor with its 4-blade baffles (SPS 37-62, Vol. III). For the RMIR-5 3-blade array both chamber and cavity modes were encountered depending on baffle length.

For baffle lengths $\leq$4.5 in. (11.43 cm), chamber modes were always observed for the unstable firings with the 3-blade array. The observed modes varied from a spinning first tangential motion at a baffle length of 1.5 in. (3.81 cm), to a standing first transverse for 2.4 in., (6.10 cm), to a standing second transverse for 2.9 in. (7.37 cm), to a first radial mode for 3.4 in. (8.64 cm), and back to a second standing transverse motion at 4.0 and 4.5 in. (10.20 and 11.43 cm) baffle lengths. Frequencies as measured by Photocons at the 4.0 in. (10.20 cm) station are summarized in Table 2. The frequency of the first tangential modes (spinning or standing) decreased with increasing baffle length, whereas no such variation was noted for the other chamber modes.

For lengths $\geq$5.0 in. (12.70 cm) only cavity modes were present. In this case, cavity 1 (Fig. 1) generally exhibited a sharp-fronted wave traveling back and forth in the transverse direction of the cavity with a nearly constant frequency of from 2255 to 2315 Hz independent of baffle lengths between 5.0 and 7.8 in. (12.70 and 19.81 cm). Intermittently, cavity 2 would often simultaneously exhibit a similar wave motion, but with a consistently lower frequency in the range of 2000 Hz. Under these conditions cavity 3 appeared very noisy and occasionally exhibited a frequency of ~4740 Hz. Phase measurements between the oscillations in the individual cavities always indicated that the cavities were uncoupled gas-dynamically. From similar measurements, no definite relationship between chamber and cavity oscillations were apparent. Finally, the chamber oscillations did not correspond with a natural chamber mode, even though the cavity frequencies were near the first tangential chamber frequency. Rather, the downstream oscillations appeared generally noisy, occasionally exhibiting all the cavity mode frequencies simultaneously; i.e., a chamber mode did not appear to be coupled to the cavity modes.

In summary, the effectiveness of baffles for stabilizing the RMIR-5 combustor can be stated as follows. The 5-blade array with length $\geq$2.9 in. (7.37 cm) provides a high margin of dynamic stability, prohibiting the development and sustenance of either cavity or chamber modes of resonance. On the other hand, the 3-blade array provides substantially less stability margin, allowing cavity modes to be sustained when the baffles were $\geq$5 in. (12.70 cm) long and failing to prevent sustained chamber modes when $\leq$4.5 in. (11.43 cm) long.

4. Comparisons With Previous Results

a. Bomb pulse amplitude and damping time. For the adequate or nearly adequate baffle configurations, it was possible to measure damping times[1] and initial pulse amplitudes. Both were found to vary (for a fixed baffle condition) with bomb size and position, and measurement location; however, average values for 3 peripheral locations were taken to be a measure of the damping behavior of the engine. Figure 2 shows typical results for the RMIR-5 and RC-1 engines. (Analogous data for the RMIR-7 engine is not available.) If it is recalled that the 3-blade array for RMIR-5 did not provide a high margin of stability, it can be seen by comparing the damping times of the 3-blade array with those of the 5-blade and RC-1 arrays that damping time per se does not provide a positive measure of stability margin when the injected flow response is minimal. For this situation, damping time appears to be highly correlated with the time constant of the chamber-nozzle combination.

b. Resonance frequency and amplitude reduction. Even though inadequate baffling fails to prohibit the development of the first transverse chamber mode, the frequency as well as the amplitude of the wave is attenuated compared to the unbaffled situation.

Frequency reduction. The reduction of frequency of the first transverse chamber mode when chamber and baffle cavity oscillations are gas-dynamically coupled is expected both from analysis and past experimental observations. However, published theoretical analysis of the phenomena are limited to two-dimensional geometries without combustion sources or sinks (Ref. 3), while at the same time published data from engine firings are fragmentary. Figure 3 shows results for the three JPL

[1]Damping time is frequently used as a measure of stability margin. As used here, this term is defined as the total time (to the nearest millisecond) for the chamber pressure from Photocon measurements at the 4.0 in. (10.20 cm) chamber station to return to its pre-disturbance appearance on a high time-resolution oscillograph record.

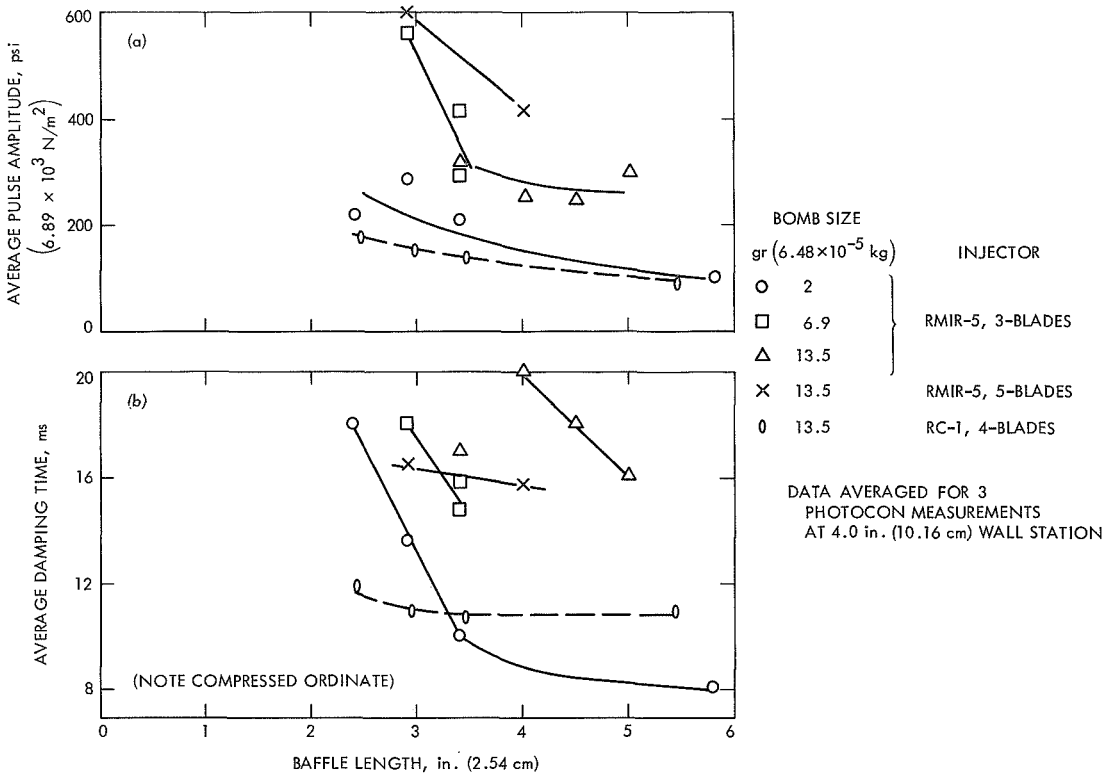

Fig. 2. Average damping time and pulse amplitude versus baffle length for injectors RMIR-5 and RC-1

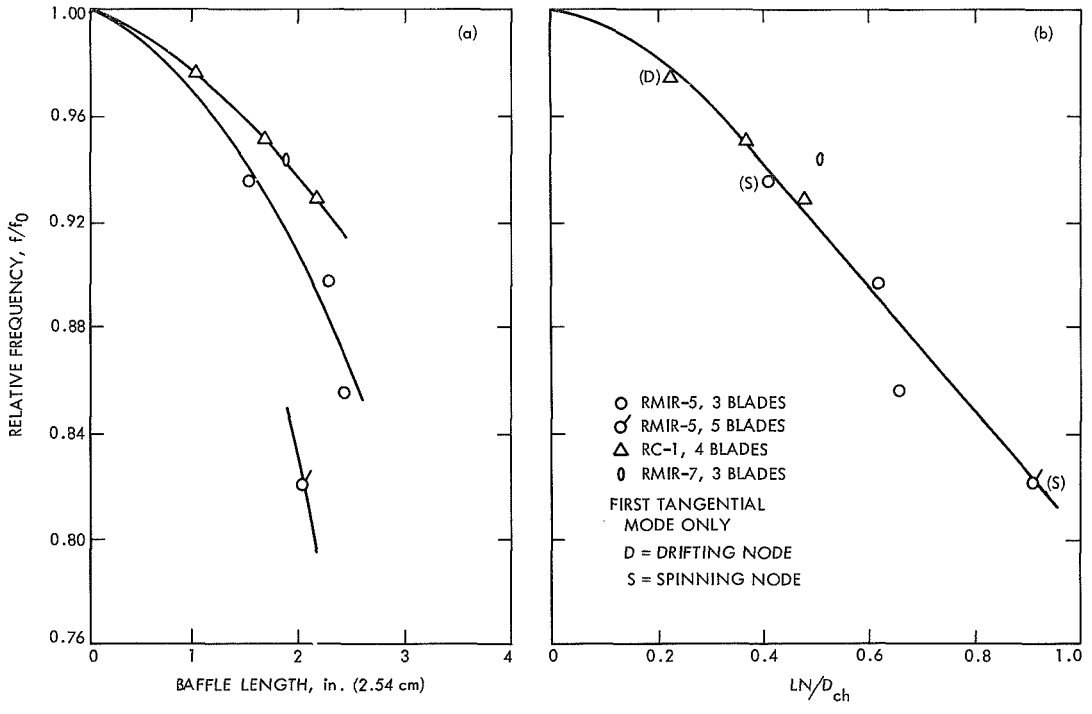

Fig. 3. Relative frequency versus baffle length and the parameter LN/D_{ch} for injectors RMIR-5, RC-1, and RMIR-7

combustors, where relative frequency f/f_0 is shown versus baffle length L (Fig. 3a), and the parameter LN/D_{ch} (Fig. 3b), where N is the number of baffle blades and D_{ch} is the chamber diameter. As indicated in Ref. 3, the relative frequency is not a function of baffle length alone. These data suggest that f/f_0 is nearly linearly related to LN/D_{ch}. Chamber length is not a significant variable in this data since all the engines had chamber lengths from injector nozzle entrance between 15.86 and 16.43 in. (40.30 and 41.70 cm). Interestingly, the reduction in frequency does not appear to be influenced by whether the mode is spinning or standing.

Amplitude reduction. The limited analytical results from Ref. 3, based on a model of pressure coupling between the chamber and the baffle cavities indicate that pressure amplitude in the cavities tends to increase relative to the amplitude for the chamber space, thus suggesting a *destabilizing* effect of baffles. No such effect has been observed in the present experimental results, nor is it generally observed by others for liquid rocket engines. Resonance amplitude variations as a function of chamber wall axial station for several lengths of baffles for the RC-1 engine are shown in Fig. 4. These results typify analogous trends for the RMIR-5 and 7 engines. The pressures were measured with Kistler transducers located near the pressure antinode of the first tangential waves; therefore, they are maximum amplitudes for each baffle condition. The amplitude distribution for the unbaffled chamber is also shown. The latter distribution was obtained for the fully developed spinning detonation-like wave, characteristic of the unbaffled engines. In addition to preventing this severely destructive mode from developing, the baffles clearly reduced the amplitude of the standing mode as their length was increased toward the 2.4 in.-length (6.10 cm) required to stabilize the RC-1 engine. Note that this length corresponds to the axial station where the slope of the unbaffled pressure distribution curve nears a minimum value.

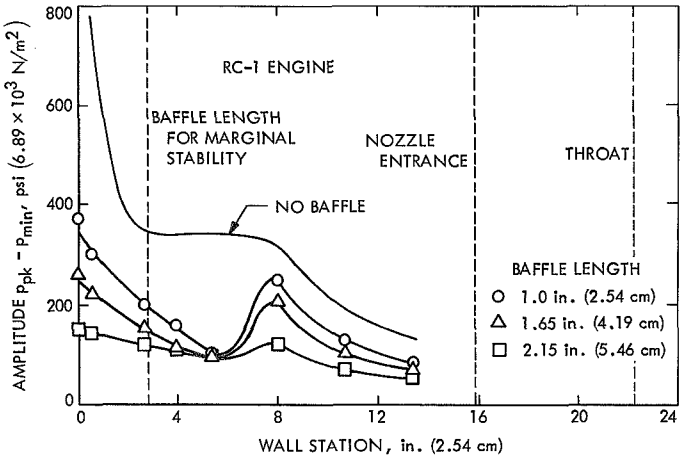

Fig. 4. Resonant pressure distribution for various baffle lengths, RC-1 engine

c. Correlation of baffle performance results. Initial comparisons of the results, particularly the apparent amplitude/critical baffle length relationship noted in Fig. 4, indicated that variations in energy and mass source distributions for each combustor must be accounted for if a correlation of stabilizing performance with baffle geometry and axial combustion distribution indeed exists. However, prior to using extensive computer calculations, based on assumed initial spray properties, to evaluate the evaporatively controlled combustion rates along the length of the combustors, it was decided to attempt a correlation of the data on the basis of existing cold flow measurements of the mass distribution produced by the specific elements used in each injector. That is, if the axial mass concentration of unreacted propellants is a first-order variable controlling baffle stabilizing effectiveness, it is reasoned that at least a partial measure of such a variable is contained in a comparison of local values of injected mass flux with the average chamber mass flux.

For this purpose, a variable termed $\mathscr{G}_{rel}$ was selected that is defined as the value of the element peak axial mass flux $(G_{max})_{L'}$ on a plane perpendicular to the chamber axis a distance L' from the impingement point divided by the average chamber mass flux, $\bar{G}_{ch}$; where L' is the axial distance of the downstream edge of the baffle from the impingement point. Thus,

$$\mathscr{G}_{rel} \equiv \frac{(G_{max})_{L'}}{\bar{G}_{ch}}$$

The evaluation of $(G_{max})_{L'}$ is based on cold flow (nonreactive fluids) measurements of the mass distributions of the particular elements, for which the experimental methods are described in Ref. 4. The essential features of the evaluation are shown in Fig. 5. Pertinent values of the sampled spray properties are listed in Table 2.

As noted previously, the RMIR-5 experiments showed a dependence of stabilizing performance on baffle spacing as well as length; therefore, any correlation of baffle effectiveness with combustion distribution must also account for this second spatial property of the baffle

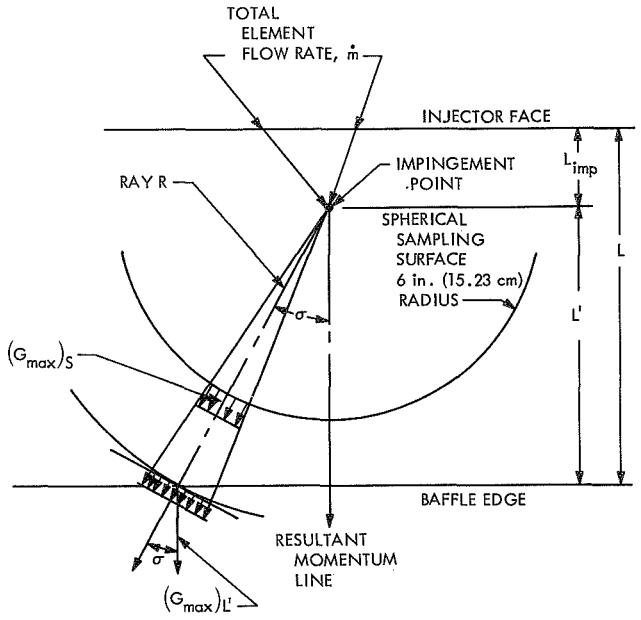

$$\mathscr{G}_{rel} \equiv \frac{(G_{max})_{L'}}{\bar{G}_{ch}}$$

WHERE FROM GEOMETRY AND CONSERVATION OF SPRAY PARTICLE MASS:

$$(G_{max})_{L'} = (G_{max})_S \frac{\dot{m}_{el}}{\dot{m}_s}\left(\frac{6}{L'}\right)^2 (\cos\sigma)^2$$

OR IF $\dfrac{(G_{max})_S}{\dot{m}_s} \equiv (G_{max})_{SN}$

THEN

$$(G_{max})_{L'} = \frac{36\,\dot{m}_{el}\,(G_{max})_{SN}\,(\cos\sigma)^2}{(L')^2}$$

$(G_{max})_S$ SAMPLED PEAK MASS FLUX ALONG RAY R

$(G_{max})_{L'}$ PEAK AXIAL MASS FLUX ON PLANE AT DISTANCE L' FROM IMPINGEMENT POINT

σ TRUE ANGLE OF RAY R

$\dot{m}_s$ TOTAL FLOW RATE DURING SAMPLING

$\dot{m}_{el}$ NEW FLOW RATE (e.g., ELEMENT FLOW RATE FOR ENGINE FIRING)

SEE TABULATED VALUES IN TABLE 2

Fig. 5. Spray mass flux relationships

array. Based primarily on heuristic arguments, different arrangements of baffle cavities can be shown to be more or less compatible with particular acoustic modes of gas motion in the unbaffled portion of the chamber. For example, Ref. 5 states that an odd number of radial blades is most effective against the tangential modes and that the order of the mode divided by the number of blades should not be an integer. However, clear evidence of a relationship of this kind has not been observed in the present results.

For the RMIR-5 engine with the 3-blade array both the first and second tangential modes were observed for particular ranges of baffle length (Table 3). For the RC-1 engine with 4 blades, only the first tangential mode was observed and the velocity nodes were not aligned with a blade but, rather, bisected opposing cavities. And for RMIR-7, the engine was equally well stabilized against the first tangential with either 3- or 4-blade arrays of adequate length. Therefore, while some relationship of baffle cavity dimension to chamber dimension is evidently important to stabilizing effectiveness, it is not clear from these data that it is strictly an acoustic mode relationship. However, for the lack of a more definitive spatial correlating parameter, one of this nature will be used.

The apparent interaction of the relative local mass flux, baffle length, and blade spacing on baffle performance for the three combustors is shown in Fig. 6. A data point for each combustor/baffle configuration is plotted as the ratio of average cavity-peripheral-width $\bar{w}$ to the first tangential wave length λ_0 versus $1/\mathscr{G}_{rel}$. The width $\bar{w}$ was taken as the chamber circumference divided by the number of radial baffles less the blade thickness, and λ_0 was based on the measured first tangential frequency for each unbaffled engine. The data are plotted as $1/\mathscr{G}_{rel}$ so that the direction of increasing L' is to the right.

Each combustor/baffle configuration was classified as stable, marginally stable, or unstable according to its observed response to combustion chamber disturbances,

Table 3. RMIR-5 dynamic stability results

Blade array	3			5
Disturbance[a]	2.0	6.9	13.5	13.5
Blade length[b], in. (2.54 cm)				
1.5	U 1T-1982 (Drifting)			
2.0				U 1TS-1735
2.4	U 1T-1812			
2.9	S	U 2T-3380		S
3.4[c]	S	U 1R-4160 S	U 1R-4160	
4.0			U 2T-3380	S
4.5			U 2T-3370	
5.0			U C1-2255	
5.8[c]	U C1-2270		U C1-2280 U C1-2270 U C1-2255	
7.8[c]			U C1-2260 U C1-2315	

[a]Numerals indicate bomb size.

[b]U, unstable; S, stable; mode designations with frequency, 1TS-first spinning tangential, 1T-first standing tangential, 2T-second standing tangential, 1R-first radial, C1-transverse mode in cavity 1.

[c]More than one classification per baffle length denotes replicate firings.

whether artificially or spontaneously imposed. A configuration was classified as stable if all disturbances damped with no discernible tendency for resonance at a sustained amplitude. Marginal stability was assigned to the engine if any discernible resonance occurred intermittently, either during a single run or a succession of runs. This classification was also assigned to engines that were sensitive to some disturbances, but insensitive to others. The unstable classification was assigned if the engine consistently exhibited continuous resonance from the time of its initiation, by whatever means, through the remainder of the firing.

As can be seen from Fig. 6, baffle configurations provided dynamic stability when blade length was sufficient to reduce $\mathscr{G}_{rel}$ to approximately 3; if, simultaneously, the number of blades was sufficient to keep $\bar{w}/\lambda_0$ below approximately 0.57. It is noted that the latter restriction is based only on the 3-blade RMIR-5 engine which exhibited higher-order chamber and cavity modes with baffle lengths beyond those required to prevent the first tangential mode. This may reflect a relatively low combustion rate for the SFNA + *Corporal* fuel propellants allowing high concentrations of unreacted propellants within the cavities. It is further noted that one stable RMIR-7 configuration (with N_2H_4) occurred to the left of the stability limit line which suggests that its combustion rate may be relatively more rapid than implied by the simple relative mass flux parameter.

Since these results were obtained for relatively large engines with a fixed contraction ratio, and since the injectors produced a relatively large thrust per element [135 to 425 lbf (600 to 1890 N)], it is of interest to compare analogous baffle performance data reported in Ref. 6 for the Rocketdyne *Apollo* lunar module (LM) ascent engine. This engine offers a contrast to the JPL research engines in that chamber diameter [7.79 in. (19.78 cm)], contraction ratio (2.9), orifice size scale (<20 lbf (89 N)/element) and orifice length ($<4D$) are significantly different. However, the impingement angle and diameter ratio of the LM unlike doublet core elements are sufficiently similar to the RC-1 element design to allow an assumption of the same values for $(G_{max})_{SN}$ and the angle σ (see Table 2 and Fig. 5) for the two elements. With this assumption and $\dot{m}_{el}$ for the LM elements,[2] it is then possible to compute $\mathscr{G}_{rel}$ for various baffle lengths. The results for the LM engine are shown in Fig. 7, where it can be seen that they are consistent with the limit lines noted for the JPL engines. This agreement is possibly fortuitous, but on the other hand, it lends credence to the applicability of the work reported here to stable-engine design.

[2]Dimensional and operational data for the LM injector was furnished by Carl L. Oberg via Rocketdyne letter 70RC10366, dated September 24, 1970.

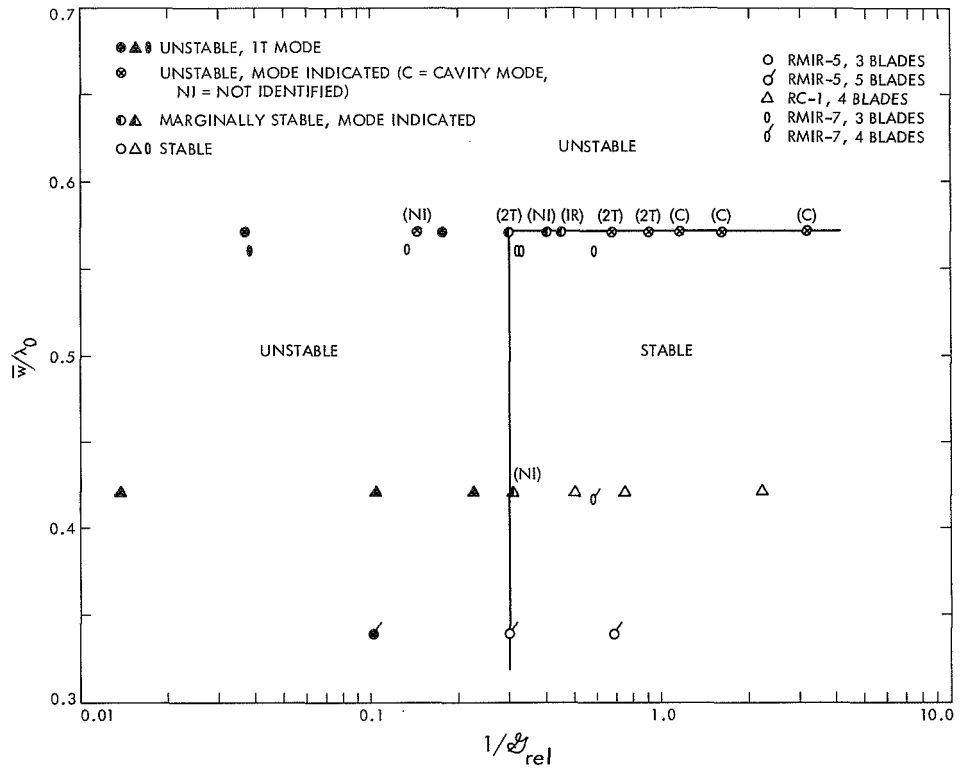

Fig. 6. $1/\mathcal{G}_{rel}$ versus $\bar{w}/\lambda_0$ for JPL research engines

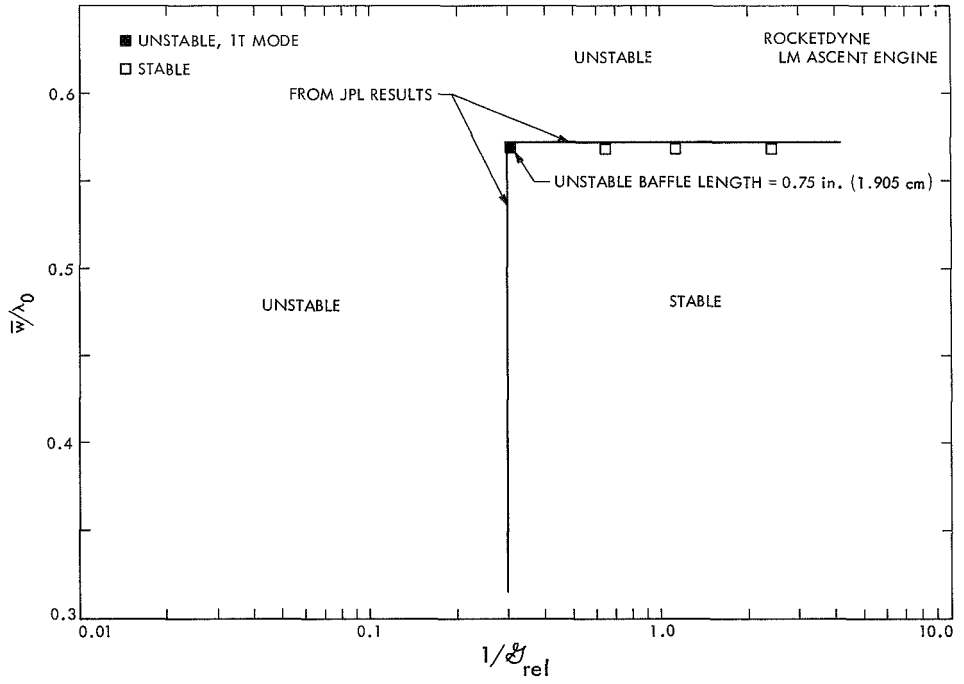

Fig. 7. $1/\mathcal{G}_{rel}$ versus $\bar{w}/\lambda_0$ for Rocketdyne *Apollo* LM engine

5. Conclusions

The baffle length required for dynamic stability is primarily controlled by the concentration of unreacted propellants in the early reaction region of the chamber.

Even though combustion rates for specific propellants and atomization conditions affect this concentration, a rudimentary design criterion is to limit the value of $\mathcal{G}_{rel}$ to 3, while at the same time limiting $\bar{w}/\lambda_0$ to less than about 0.57 by using at least three baffle blades.

In order to assure reproducible stability, sufficient hydraulic control of the injection scheme must be exercised to maintain the critical spatial relationship between a fixed baffle geometry and the unreacted propellant distribution under perturbed chamber conditions. The lower limit of control sufficiency remains to be determined.

References

1. Clayton, R. M., Rogero, R. S., and Sotter, J. G., *An Experimental Description of Destructive Liquid Rocket Resonant Combustion,* Technical Report 32-1293, Jet Propulsion Laboratory, Pasadena, Calif. (Reprinted from *AIAA Journal,* Vol. 6, No. 7, pp. 1252–1259, July 1968).

2. Rupe, J. H., *An Experimental Correlation of the Nonreactive Properties of Injection Schemes and Combustion Effects in a Liquid-Propellant Rocket Engine: Part V. On the Influence of Vanes on Combustion and Combustion Stability,* Technical Report 32-255, Jet Propulsion Laboratory, Pasadena, Calif., Sept. 15, 1967.

3. Oberg, C. L., Wong, T. L., and Schmeltzer, R. A., *Analysis of the Acoustic Behavior of Baffled Combustion Chambers,* Report R-8076 (NASA CR-72625), North American Rockwell Corporation, Rocketdyne Division, Canoga Park, Calif., January 1970.

4. Rupe, J. H., *An Experimental Correlation of the Non-reactive Properties of Injection Schemes and Combustion Effects in a Liquid Propellant Rocket Engine: Part I. The Application of Nonreactive-Spray Properties to Rocket-Motor Injector Design,* Technical Report 32-255, Jet Propulsion Laboratory, Pasadena, Calif., July 15, 1965.

5. *Design Guide for Stable H_2/O_2 Combustors: Volume 1. Design Application,* Report 20672-P2D, Aerojet Liquid Rocket Company, Sacramento, Calif., May 1970.

6. *Lunar Module Ascent Engine Acoustic Cavity Study,* Report R-7935, North American Rockwell Corporation, Rocketdyne Div., Canoga Park, Calif., Aug. 1, 1969.

7. Knight, R. M., Nurick, W. H., *Correlation of Spray Dropsize Distribution and Injector Variables,* Interim Report, R-7995, North American Rockwell Corporation, Rocketdyne Div., Canoga Park, Calif., Sept. 30, 1969.